Hindawi
Advances in Civil Engineering
Volume 2022, Article ID 9184338, 15 pages
https://doi.org/10.1155/2022/9184338

Research Article

Semianalytical Solution for Thermal Consolidation of Viscoelastic Marine Clay with the Fractional Order Derivative

Minjie Wen,[1,2] Lichen Li,[3] Xinchen Qiu,[2] Yi Tian,[3] Kuihua Wang,[2] Kaifu Liu,[1] and Wenbing Wu[2,3]

[1]*School of Civil Engineering and Architecture, Zhejiang Sci-Tech University, Hangzhou, Zhejiang 310018, China*
[2]*Research Center of Coastal Urban Geotechnical Engineering, Zhejiang University, Hangzhou, Zhejiang 310058, China*
[3]*Faculty of Engineering, Zhejiang Institute, China University of Geosciences, Wuhan, Hubei 430074, China*

Correspondence should be addressed to Wenbing Wu; zjuwwb1126@163.com

Received 16 May 2022; Accepted 7 June 2022; Published 29 June 2022

Academic Editor: Pengjiao Jia

The deformation property of marine clay under a heat source has received considerable attention in the geotechnical literature. In this paper, a three-parameter fractional order derivative model is introduced into the thermo-hydro-mechanical coupling governing equations with thermal filtration and thermo-osmosis to simulate viscoelastic characteristics of marine clay. The excess pore pressure, temperature increment, and displacement of marine clay are derived by using the Laplace transform method, and the semianalytical solution for the one-dimensional thermal consolidation in the time domain is derived by using a numerical inversion of the inverse Laplace transform. The influence of the order of the fractional derivative, material parameters, and phenomenological coefficient on thermal consolidation is investigated based on the present solutions. It is shown that the influence of the fractional derivative parameter on the excess pore pressure and displacement of marine clay depends on the properties of soil mass, and the temperature increment has an obvious effect on the thermal filtration and thermo-osmosis process.

1. Introduction

Over the past decades, more and more engineering activities have caused the change in the temperature field of the surrounding soil layers, which inevitably affects the physical and mechanical properties of the strata. These engineering activities involve a broad range of civil engineering topics such as deep geological disposal of radioactive waste [1], deep drilling and excavation [2, 3], extraction of geothermal energy [4–6], energy piles [7, 8], ground improvement using prefabricated vertical thermal drain [9–11], oil and gas pipelines [12], and frictional heating-induced large-scale landslides [13]. This huge engineering demand has stimulated scholars to pay their attention on the thermo-hydro-mechanical coupling theory of porous media, especially the deformation properties of marine clay under a heat source [14].

Biot originally proposed the constitutive equations considering the thermal effect and established the theoretical framework for the thermodynamics of saturated porous media [15]. Following Biot's research, a number of scholars have investigated the thermal consolidation of elastic saturated porous media by considering the influence of the thermal effect. Booker and Savvidou studied the thermal consolidation of saturated soil under the action of the deep buried spherical and point heat source [16, 17]. Bai [18] derived an analytical solution for the wave response of porous materials under cyclic thermal load [18]. Smith and Booker [19] established the linear thermoelastic theory of homogeneous isotropic materials by using the Green function method [19]. Lu et al. [20] investigated the thermal-mechanical coupling response of saturated porous media under simple harmonic heat and load based on the generalized thermoelastic theory [20]. Ai and Wang [21] studied the axisymmetric thermal consolidation of layered elastic saturated porous media under the action of the heat source [21]. Furthermore, Ai et al. [22] studied the axisymmetric thermal consolidation of layered transversely isotropic

porous media [22]. Wen et al. [23] studied the thermal dynamic response of a lined circular tunnel in saturated elastic porous media with the help of a fractional order derivative [23].

Although the above-mentioned scholars have greatly promoted the development of the thermo-hydro-mechanical coupling theory of porous media, they neglect thermal filtration (the influence of the excess pore pressure gradient on heat flux) and thermo-osmosis (the influence of the temperature gradient on water flux). In reality, by conducting an experiment on thermo-osmosis of water through kaolinite, Srivastava and Avasthi [24] found that the water flux associated with thermo-osmosis in compacted kaolinite can reach 10^{-8} m/s under a temperature gradient of 20°C/m [24]. Considering the influence of thermal filtration and thermo-osmosis, Zhou et al. [25] presented a fully coupled thermo-hydro-mechanical model [25]. Considering the influence of seepage velocity on thermal diffusion and the temperature gradient on seepage velocity, Liu et al. [26] established a fully dynamic coupled thermo-hydro-mechanical model and investigated the influence of the thermal and water permeability coefficient of saturated porous media around cylindrical holes and spherical cavities on their thermodynamic response, respectively [26, 27]. Yang et al. [25] proposed a refined mathematical model to study the coupled effect of thermo-osmosis in saturated porous media [28]. All these references utilized the elastic theory to simulate stress-strain relationships in saturated porous media, which may not be applicable to the marine clay covering two-thirds of the Earth.

With the continuous development of marine development all over the world, more and more attention has been paid to the deformation characteristics of marine clay. Liu et al. [29] studied the one-dimensional consolidation of viscoelastic marine soft soil under load varying with depth and time [29]. Liu et al. [14] investigated the effect of viscosity on the one-dimensional thermal consolidation of marine soft soil [14]. Wang and Wang [30] studied the rheology and thermal consolidation of layered saturated soft soil under force and thermal load [30]. Although these works have promoted the understanding of the deformation characteristics of marine clay, the existing research is still far from being applied to the engineering applications in marine clay due to its complex rheological properties. In order to reasonably consider the rheological characteristics of soil, many scholars introduced the fractional constitutive model to study the consolidation characteristics of soil [31–35]. However, to the authors' knowledge, there is no report on the thermal consolidation of viscoelastic marine soil with a fractional order derivative.

In light of the above, the objective of this paper is to investigate the one-dimensional thermal consolidation of viscoelastic marine clay with the fractional order derivative. By introducing a three-parameter fractional order derivative model to consider thermal filtration and thermo-osmosis, the solutions of excess pore pressure, temperature increment, and displacement of viscoelastic marine clay are obtained by using the Laplace transform method and its numerical inverse transform. Based on the present solutions, the influence of the order of the fractional derivative, material parameters, and phenomenological coefficient on the thermal consolidation of viscoelastic marine clay is investigated.

2. Mathematical Modeling

Considering the effects of thermal filtration and thermo-osmosis, a fully coupled thermo-hydro-mechanical model was proposed by Zhou et al. [25]. On this basis, a three-parameter fractional order derivative model, consisting of two springs and one dashpot in parallel, is introduced into the thermo-hydro-mechanical coupling governing equations. The constitutive relationship of the fractional order derivative model is expressed as [36]

$$\left(1+\tau_{\varepsilon}^{\alpha}D^{\alpha}\right)\sigma'(z,t)=\left(1+\tau_{\sigma}^{\alpha}D^{\alpha}\right)(\lambda+2G)\frac{\partial u(z,t)}{\partial z}. \tag{1}$$

Here, $\sigma'(z,t)$ denotes the vertical effective stress; λ and G are Lame constants; z represents the depth below the ground surface; t is time; τ_{ε}, and τ_{σ} are material parameters; and α is the fractional order parameter which can be obtained by the triaxial test and parameter inversion method, and $0<\alpha<1$; $u(z,t)$ is the displacement in the z direction. $D^{\alpha}=d^{\alpha}/dt^{\alpha}$ denotes α order Riemann–Liouville fractional derivative, and it is defined as [36]

$$D^{\alpha}[x(t)]=\frac{1}{\Gamma(1-\alpha)}\frac{\mathrm{d}}{\mathrm{d}t}\int_{0}^{t}\frac{x(\tau)}{(t-\tau)^{\alpha}}\,\mathrm{d}\tau. \tag{2}$$

Here, $\Gamma(\varphi)=\int_{0}^{\infty}t^{\varphi-1}e^{-\varphi}\mathrm{d}t$ is the Gamma function.

As shown in Figure 1, both the top and bottom surfaces are set as permeable. Instantaneous compressive stress q_0 and temperature T_1 are applied at the top surface, and a constant temperature T_0 is maintained at the bottom surface.

The viscoelastic characteristics of marine clay are simulated by the three-parameter fractional order derivative model, the equilibrium equation is given by [25]

$$\xi p+K'\beta T-\sigma'=q_0. \tag{3}$$

Here, $\xi=1-K'/K_s$ depends on the compressibility of the soil grains; K' represents the drained bulk modulus of the soil medium; K_s denotes the bulk modulus of the soil grains; β is the coefficient of volumetric expansion of the soil medium and T is the temperature increment; and p is excess pore pressure.

Substituting equation (1) into equation (3) yields

$$\xi p+K'\beta T-\frac{1+\tau_{\sigma}^{\alpha}D^{\alpha}}{1+\tau_{\varepsilon}^{\alpha}D^{\alpha}}(\lambda+2G)\frac{\partial u}{\partial z}=q_0. \tag{4}$$

The fluid mass balance is governed by

$$k\frac{\partial^2 p}{\partial z^2}+S_w\frac{\partial^2 T}{\partial z^2}=c_1\frac{\partial^2 u}{\partial z\partial t}-c_2\frac{\partial T}{\partial t}+c_3\frac{\partial p}{\partial t}. \tag{5}$$

Here, k denotes the coefficient of permeability; S_w is a phenomenological coefficient associated with the influence of the thermal gradient on the water flux (thermo-osmosis); the parameters c_1, c_2, and c_3 are expressed as $c_1=1-K'/K_s$,

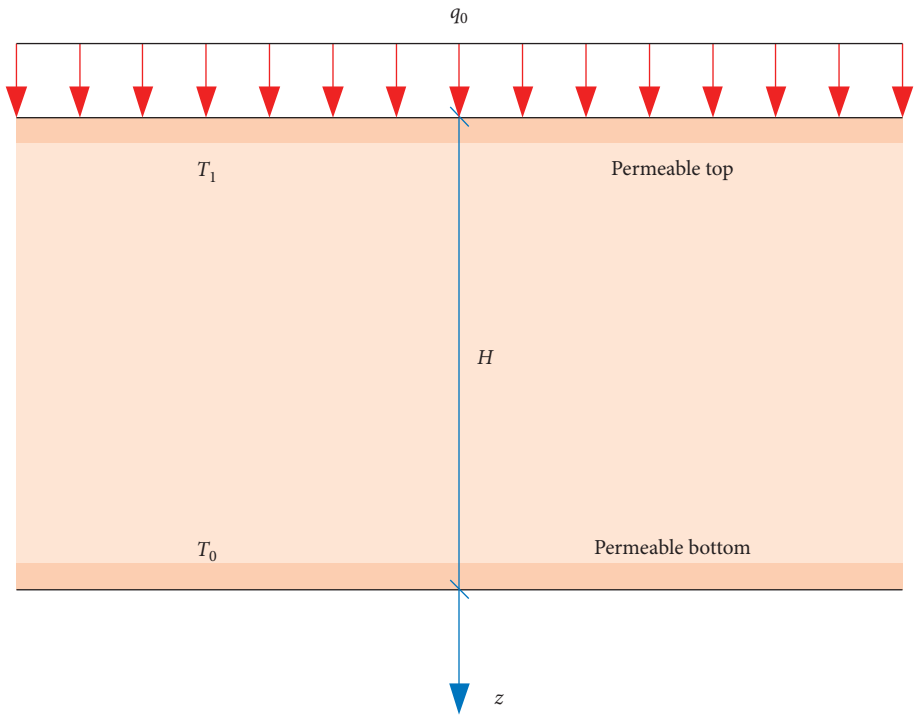

Figure 1: Mathematical model.

$c_2 = na_w + (1-n)a_s - \beta K'/K_s$, and $c_3 = n/\beta_w - (1-n)/K_s$, respectively; n is the porosity; a_w and a_s are volumetric thermal expansion coefficients of the pore water and soil grains, respectively; and β_w is the bulk modulus of pore water.

The thermal energy balance equation is given as

$$C_v\frac{\partial T}{\partial t} - T_0K'\beta\frac{\partial^2 u}{\partial z\partial t} = \left(K - T_0a_w\beta_wS_w\right)\frac{\partial^2 T}{\partial z^2} + T_0\left(S_w - a_w\beta_wk\right)\frac{\partial^2 p}{\partial z^2}, \tag{6}$$

where C_v is the volumetric specific heat of the soil medium; $C_v = (1-n)\rho_sC_s + n\rho_wC_w$; ρ_s is the density of soil grains; ρ_w is the density of water; C_s and C_w denote the gravimetric specific heats of soil grains and the pore water, respectively; and $K = (1-n)\lambda_s + n\lambda_w$ is the thermal conductivity of the soil medium, in which λ_s and λ_w are the thermal conductivities of the soil grain and the pore water.

The initial conditions of the problem are as follows:

$$\begin{aligned} p(z,0) &= q_0, \\ u(z,0) &= 0, \\ T(z,0) &= 0. \end{aligned} \tag{7}$$

The boundary conditions of the problem are as follows:

$$p(0,t) = 0. \tag{8}$$

$$p(H,t) = 0. \tag{9}$$

$$u(H,t) = 0. \tag{10}$$

$$T(0,t) = T_1. \tag{11}$$

$$T(H,t) = 0. \tag{12}$$

3. Solutions to Governing Equations

Laplace transform is introduced to solve governing equations (4)–(6), and the following Laplace transform equation is defined:

$$s^\gamma\overline{f}(s) = \int_0^\infty \frac{\partial^\gamma f(t)}{\partial t^\gamma}e^{-st}\mathrm{d}t. \tag{13}$$

Applying Laplace transforms to equations (4)–(6), one can obtain transformed governing equations as

$$\xi\overline{p} + K'\beta\overline{T} - \frac{1+\tau_\sigma^\alpha s^\alpha}{1+\tau_\varepsilon^\alpha s^\alpha}(\lambda+2G)\frac{\partial\overline{u}}{\partial z} = \frac{q_0}{s}. \tag{14}$$

$$k\frac{\partial^2\overline{p}}{\partial z^2} + S_w\frac{\partial^2\overline{T}}{\partial z^2} = sc_1\frac{\partial\overline{u}}{\partial z} - sc_2\overline{T} + c_3\left(s\overline{p} - q_0\right). \tag{15}$$

$$C_vs\overline{T} - T_0K'\beta s\frac{\partial\overline{u}}{\partial z} = \left(K - T_0a_w\beta_wS_w\right)\frac{\partial^2\overline{T}}{\partial z^2} + T_0\left(S_w - a_w\beta_wk\right)\frac{\partial^2\overline{p}}{\partial z^2}. \tag{16}$$

Here, s is the Laplace transform parameter; $\overline{p} = \int_0^\infty e^{-st}p\,\mathrm{d}t$, $\overline{T} = \int_0^\infty e^{-st}T\,\mathrm{d}t$, and $\overline{u} = \int_0^\infty e^{-st}u\,\mathrm{d}t$.

The Laplace transform of equations (8)–(12) with respect to the time variable t is derived as

$$\overline{p}|_{z=0} = 0. \tag{17}$$

$$\overline{p}|_{z=H} = 0. \tag{18}$$

$$\overline{u}|_{z=H} = 0. \tag{19}$$

$$\overline{T}|_{z=0} = \frac{T_1}{s}. \tag{20}$$

$$\overline{T}|_{z=H} = 0. \tag{21}$$

Substituting equation (15) into equation (16) yields

$$a_1\frac{\partial^2\overline{T}}{\partial z^2} + a_2\frac{\partial^2\overline{p}}{\partial z^2} + a_3 s\overline{T} + a_4 s\overline{p} - a_4 q_0 = 0. \tag{22}$$

Here, $a_1 = -T_0K'\beta S_w/c_1 - K + T_0a_w\beta_w S_w$; $a_2 = -T_0K'\beta k/c_1 - T_0(S_w - a_w\beta_w k)$; $a_3 = C_v - T_0K'\beta c_2/c_1$; and $a_4 = T_0K'\beta c_3/c_1$.

Substituting equation (15) into equation (14) gives

$$b_1\frac{\partial^2\overline{T}}{\partial z^2} + b_2\frac{\partial^2\overline{p}}{\partial z^2} + b_3 s\overline{T} + b_4 s\overline{p} + b_5 q_0 = 0, \tag{23}$$

where $b_1 = 1 + \tau_\sigma^\alpha s^\alpha/1 + \tau_\varepsilon^\alpha s^\alpha(\lambda + 2G)S_w/c_1$; $b_2 = 1 + \tau_\sigma^\alpha s^\alpha/1 + \tau_\varepsilon^\alpha s^\alpha(\lambda + 2G)k/c_1$; $b_3 = 1 + \tau_\sigma^\alpha s^\alpha/1 + \tau_\varepsilon^\alpha s^\alpha(\lambda + 2G)c_2/c_1 - K'\beta$; $b_4 = -\xi - 1 + \tau_\sigma^\alpha s^\alpha/1 + \tau_\varepsilon^\alpha s^\alpha(\lambda + 2G)c_3/c_1$; and $b_5 = 1 + \tau_\sigma^\alpha s^\alpha/1 + \tau_\varepsilon^\alpha s^\alpha(\lambda + 2G)c_3/c_1 + 1$.

Further transformation of equations (22) and (23) leads to

$$\overline{T} = \frac{h_1}{s}\frac{\partial^2\overline{p}}{\partial z^2} + h_2\overline{p} + h_3\frac{q_0}{s}, \tag{24}$$

where $h_1 = a_2b_1 - a_1b_2/a_1b_3 - a_3b_1$; $h_2 = a_4b_1 - a_1b_4/a_1b_3 - a_3b_1$; and $h_3 = -a_4b_1 + a_1b_5/a_1b_3 - a_3b_1$.

Substituting equation (24) into equation (22) yields

$$g_1\frac{\partial^4\overline{p}}{\partial z^4} + g_2 s\frac{\partial^2\overline{p}}{\partial z^2} + g_3 s^2\overline{p} + \frac{s}{a_1}(a_3h_3 - a_4)q_0 = 0, \tag{25}$$

where $g_1 = h_1$; $g_2 = h_2 + a_2/a_1 + a_3h_1/a_1$; and $g_3 = a_3h_2 + a_4/a_1$.

The general solution of equation (25) is derived as

$$\overline{p} = A_1e^{\gamma_1 z} + A_2e^{-\gamma_1 z} + B_1e^{\gamma_2 z} + B_2e^{-\gamma_2 z} - \frac{a_3h_3 - a_4}{a_1g_3s}q_0, \tag{26}$$

where A_1, A_2, B_1, B_2 are undetermined coefficients.$\gamma_1^2 = -g_2 - \sqrt{g_2^2 - 4g_1g_3}/2g_1s$;$\gamma_2^2 = -g_2 + \sqrt{g_2^2 - 4g_1g_3}/2g_1s$

Substituting equation (26) into equation (24) gives

$$\begin{aligned}\overline{T} = {} & \left(\frac{h_1\gamma_1^2}{s} + h_2\right)(A_1e^{\gamma_1 z} + A_2e^{-\gamma_1 z}) + \left(\frac{h_1\gamma_2^2}{s} + h_2\right)(B_1e^{\gamma_2 z} + B_2e^{-\gamma_2 z}) \\ & - \frac{h_2(a_3h_3 - a_4)}{a_1g_3s}q_0 + \frac{h_3q_0}{s}\end{aligned}. \tag{27}$$

Substituting equation (26) into equations (17), (18), (20), and (21), the undermined coefficients can be obtained as

$$\begin{aligned}
A_1 &= -\frac{s(\phi_1 - c_{22}\phi_0)\left(1 - e^{-\gamma_1 H}\right) + T_1e^{-\gamma_1 H}}{s(c_{11} - c_{22})\left(e^{\gamma_1 H} - e^{-\gamma_1 H}\right)}, \\
A_2 &= \frac{s(\phi_1 - c_{22}\phi_0)\left(1 - e^{\gamma_1 H}\right) + T_1e^{\gamma_1 H}}{s(c_{11} - c_{22})\left(e^{\gamma_1 H} - e^{-\gamma_1 H}\right)}, \\
B_1 &= \frac{s(\phi_1 - c_{11}\phi_0)\left(1 - e^{-\gamma_2 H}\right) + T_1e^{-\gamma_2 H}}{s(c_{11} - c_{22})\left(e^{\gamma_2 H} - e^{-\gamma_2 H}\right)}, \\
B_2 &= -\frac{s(\phi_1 - c_{11}\phi_0)\left(1 - e^{\gamma_2 H}\right) + T_1e^{\gamma_2 H}}{s(c_{11} - c_{22})\left(e^{\gamma_2 H} - e^{-\gamma_2 H}\right)},
\end{aligned} \tag{28}$$

where $c_{11} = h_1\gamma_1^2/s + h_2$, $c_{22} = h_1\gamma_2^2/s + h_2$, $\varphi_0 = -a_3 h_3 - a_4/a_1 g_3 s q_0$, and $\varphi_1 = -(h_2(a_3h_3 - a_4)/a_1 g_3 s - h_3/s)q_0$.

Then, equation (26) can be rewritten as

$$\begin{aligned}\overline{p} &= -\frac{\theta_1 \sinh[\gamma_1 z] - [T_1 - \theta_1]\sinh[\gamma_1(H-z)] - T_0 \sinh[\gamma_1 z]}{h_1\left(\gamma_1^2 - \gamma_2^2\right)\sinh[\gamma_1 H]} \\ &+\frac{\theta_2 \sinh[\gamma_2 z] + [\theta_2 - T_1]\sinh[\gamma_2(H-z)] - T_0 \sinh[\gamma_2 z]}{h_1\left(\gamma_1^2 - \gamma_2^2\right)\sinh[\gamma_2 H]} + \phi_0\end{aligned}. \tag{29}$$

where, $\theta_1 = s(\varphi_1 - \varphi_0 c_{22})$ and $\theta_2 = s(\varphi_1 - \varphi_0 c_{11})$.

Substituting equations (26) and (27) into equation (14) yields

$$\begin{aligned}\frac{\partial \overline{u}}{\partial z} &= \chi\left[K'\beta\left(\frac{h_1\gamma_1^2}{s} + h_2\right) + \xi\right]\left(A_1 e^{\gamma_1 z} + A_2 e^{-\gamma_1 z}\right) + \chi\left[K'\beta\left(\frac{h_1\gamma_2^2}{s} + h_2\right) + \xi\right]\left(B_1 e^{\gamma_2 z} + B_2 e^{-\gamma_2 z}\right) \\ &+\chi q_0\left[-\frac{\xi(a_3h_3 - a_4)}{a_1 g_3 s} - \frac{K'\beta h_2(a_3h_3 - a_4)}{a_1 g_3 s} + \frac{K'\beta h_3 - 1}{s}\right]\end{aligned}, \tag{30}$$

where $\chi = 1/\lambda + 2G1 + \tau_\epsilon^\alpha s^\alpha / 1 + \tau_\sigma^\alpha s^\alpha$.

Integrating both sides of equation (30) from zero to infinity gives

$$\begin{aligned}\overline{u} &= \frac{\chi}{\gamma_1}\left[K'\beta\left(\frac{h_1\gamma_1^2}{s} + h_2\right) + \xi\right]\left(A_1 e^{\gamma_1 z} - A_2 e^{-\gamma_1 z}\right) + \frac{\chi}{\gamma_2}\left[K'\beta\left(\frac{h_1\gamma_2^2}{s} + h_2\right) + \xi\right]\left(B_1 e^{\gamma_2 z} - B_2 e^{-\gamma_2 z}\right) \\ &+\chi q_0\left[-\frac{\xi(a_3h_3 - a_4)}{a_1 g_3 s} - \frac{K'\beta h_2(a_3h_3 - a_4)}{a_1 g_3 s} + \frac{K'\beta h_3 - 1}{s}\right]z + D_1\end{aligned}. \tag{31}$$

Substituting equation (31) into equation (19), the coefficient D_1 can be obtained as

$$\begin{aligned}D_1 &= \frac{-\chi}{\gamma_1}\left[K'\beta\left(\frac{h_1\gamma_1^2}{s} + h_2\right) + \xi\right]\left(A_1 e^{\gamma_1 H} - A_2 e^{-\gamma_1 H}\right) - \frac{\chi}{\gamma_2}\left[K'\beta\left(\frac{h_1\gamma_2^2}{s} + h_2\right) + \xi\right]\left(B_1 e^{\gamma_2 H} - B_2 e^{-\gamma_2 H}\right) \\ &-\chi q_0\left[-\frac{\xi(a_3h_3 - a_4)}{a_1 g_3 s} - \frac{K'\beta h_2(a_3h_3 - a_4)}{a_1 g_3 s} + \frac{K'\beta h_3 - 1}{s}\right]H\end{aligned}. \tag{32}$$

Through the above derivation, the analytical expressions of excess pore pressure, temperature increment, and displacement can be obtained accordingly. However, it is difficult to directly obtain the analytical solutions in the transformed space for some formulas are difficult to integrate. Therefore, it is necessary to utilize the numerical method to program and analyze the solution process in this paper. Currently, there exist many Laplace inverse transform methods, among which the Crump's numerical inversion results of Laplace transform is the most accurate [10].

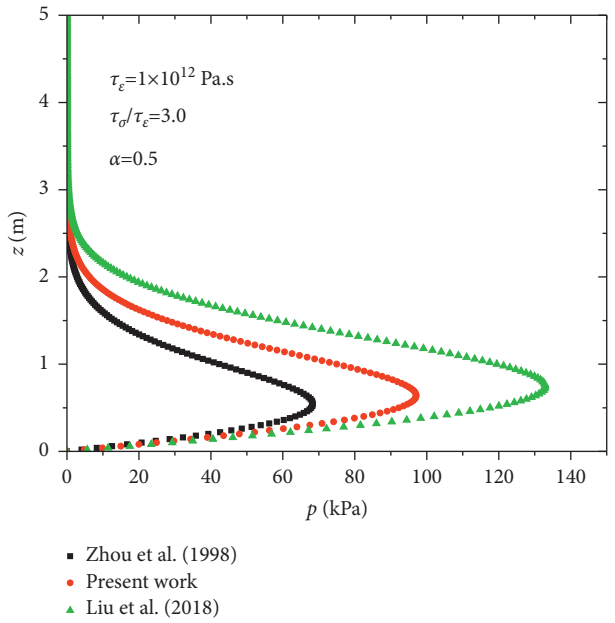

Figure 2: Comparison of excess pore pressure among solutions of Zhou et al. [25], Liu et al. [14], and present work.

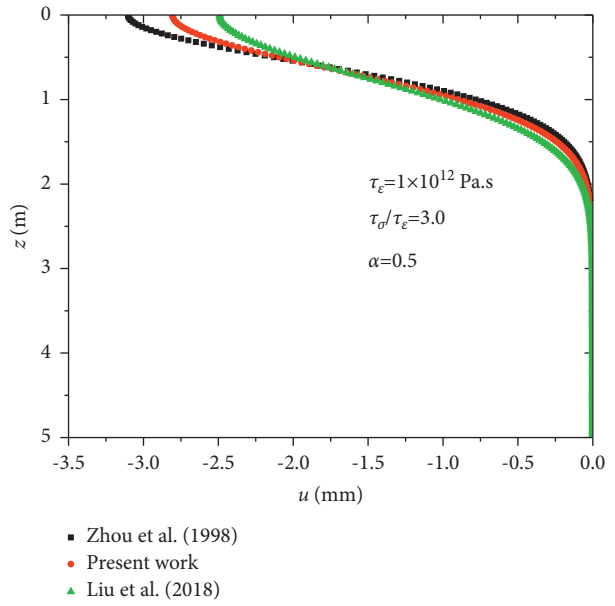

Figure 3: Comparison of displacement among solutions of Zhou et al. [25], Liu et al. [14], and present work.

Assuming that $F(s)$ is the Laplace transform of function $F(t)$, Crump's inversion algorithm of the Laplace inverse transform can be written as

$$F(t) \approx \frac{e^{at}}{T^*}\left\{\frac{1}{2}F(a) + \sum_{m=1}^{500}\left[\mathrm{Re}\left[F\left(a+\frac{m\pi i}{T^*}\right)\right]\cos\frac{m\pi t}{T^*} - \mathrm{Im}\left[F\left(a+\frac{m\pi i}{T^*}\right)\right]\sin\frac{m\pi t}{T^*}\right]\right\}, \tag{33}$$

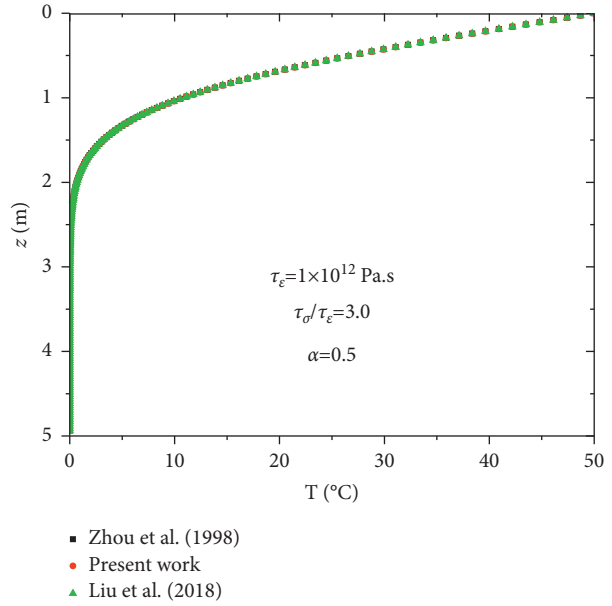

Figure 4: Comparison of temperature increment among solutions of Zhou et al. [25], Liu et al. [14], and present work.

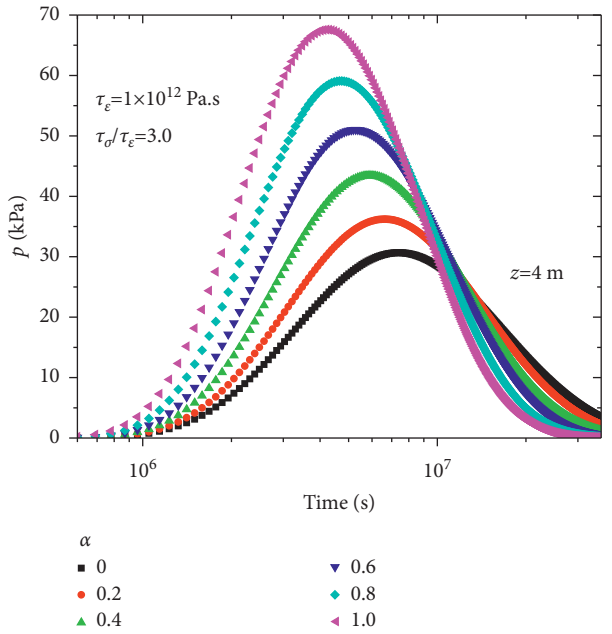

Figure 5: Influence of the order of the fractional derivative on excess pore pressure when $\tau_\sigma/\tau_\varepsilon = 3$.

where $T^* > t/2$. If $|F(t)| < Me^{\alpha t}$, the error $|\varsigma| \leq Me^{\upsilon} e^{-2T^*(a-\upsilon)}$.

4. Numerical Results and Discussion

Having illustrated and reviewed the obtained theoretical results in the preceding section, we now present some numerical results. Following the works of Liu et al. [14] and Zhou et al. [25], the parameters of marine clay in the calculation can be set as $\lambda = 6 \times 10^6$ Pa, $G = 8 \times 10^6$, $n = 0.25$, $S_w = 6.0 \times 10^{-11}$ m^2/s/°C, $K' = 2.78 \times 10^6$ Pa, $k = 1.0 \times 10^{-14}$ m^5/J/s, $\lambda_w = 0.582$ J/m/s/°C, $\lambda_s = 3.29$ J/m/s/°C, $K_s = 59 \times 10^9$ Pa, $\beta_w = 3.3 \times 10^9$ Pa, $\rho_w = 1000$ kg/m^3, $\rho_s = 2610$ kg/m^3, $C_w = 4186$ J/kg/°C, $C_s = 937$ J/kg/°C, $a_s = 3.0 \times 10^{-6}$°C^{-1}, $a_w = 3.0 \times 10^{-4}$°C^{-1}, $\tau_\varepsilon = 1 \times 10^{12}$ Pa · s, $q_0 = 0$ Pa, $T_1 = 50$°C, and $T_0 = 23$°C.

4.1. Comparative Analysis. The Kelvin viscoelastic model is combined with the thermo-hydro-mechanical coupling governing equations for marine clay, and the influence of viscosity on one-dimensional thermal consolidation was

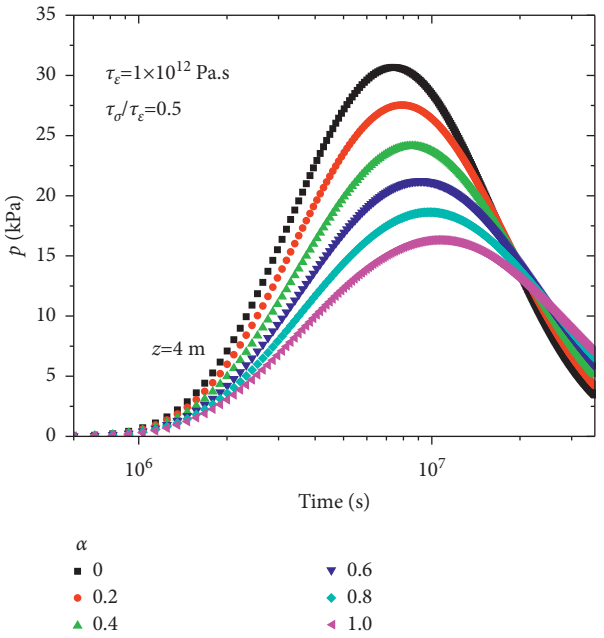

Figure 6: Influence of the order of the fractional derivative on excess pore pressure when $\tau_\sigma/\tau_\varepsilon = 0.5$.

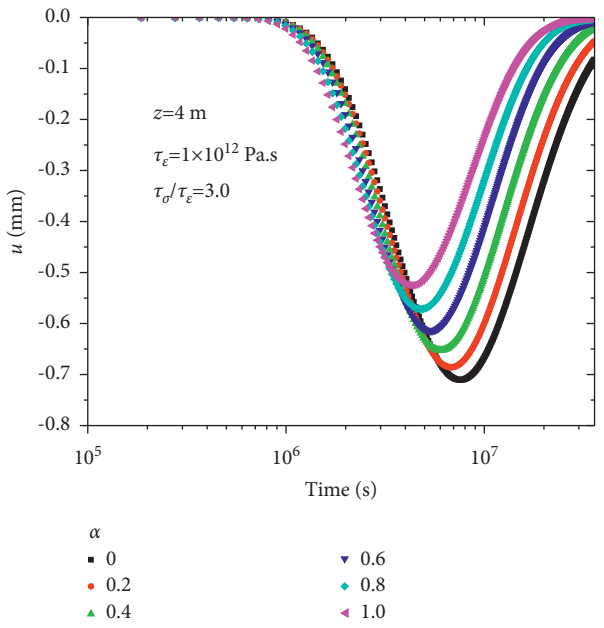

Figure 7: Influence of the order of the fractional derivative on displacement when $\tau_\sigma/\tau_\varepsilon = 3$.

investigated by Liu et al. [14]. In addition, Zhou et al. [25] proposed a fully coupled thermo-hydro-mechanical model with thermal filtration and thermo-osmosis. In this paper, for the purpose of verifying and presenting the differences of the three cases of the fractional derivative viscoelastic model (FDVM), Kelvin viscoelastic model (KVM), and elastic model (EM), the order of the fractional derivative α is assumed to be zero for the comparison of the FDVM with the EM, and the material parameter τ_ε^α is assumed to be zero, and α is equal to 1 for the comparison of the FDVM with the KVM. Figures 2–4 illustrate the distribution of excess pore pressure, displacement, and temperature increment against depth among solutions of Zhou et al. [25], Liu et al. [14], and present work. It can be found that the KVM produces the largest excess pore pressure, followed by the results of the FDVM and EM. At depth above 0.6 m, the displacement value produced by the EM is the largest, followed by those of the FDVM and KVM. At larger depth, remarkable increase

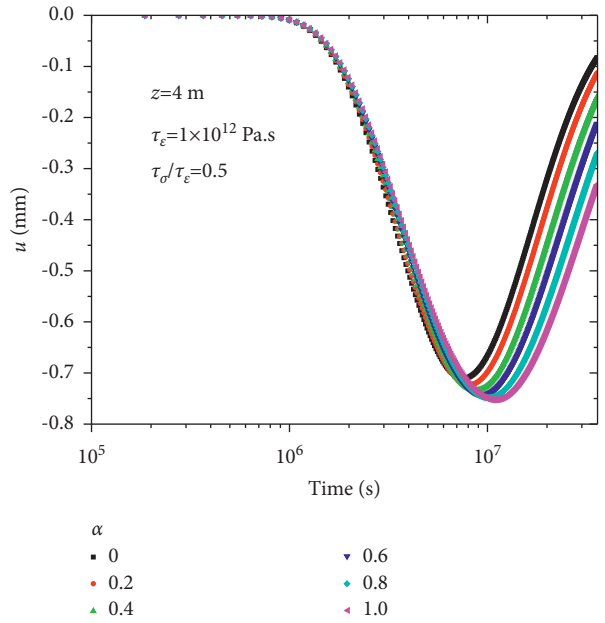

Figure 8: Influence of the order of the fractional derivative on displacement when $\tau_\sigma/\tau_\varepsilon = 0.5$.

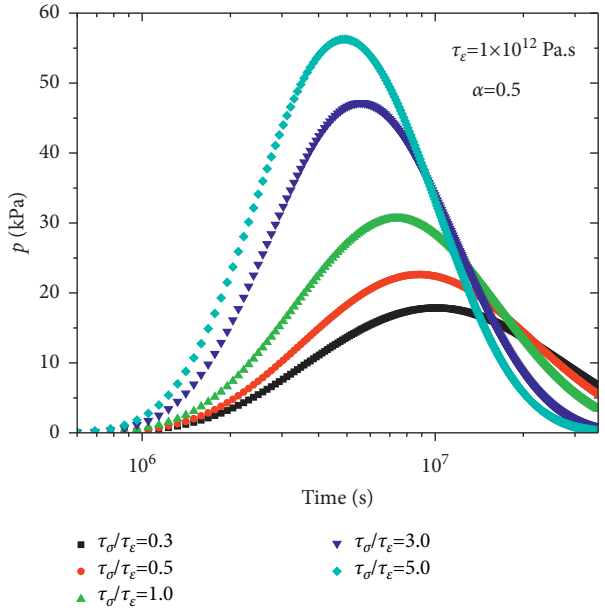

Figure 9: Influence of the material parameter $\tau_\sigma/\tau_\varepsilon$ on excess pore water pressure when $\alpha = 0.5$.

of the displacement value could be observed for all the three models. For the distribution of temperature, the three models produce similar results.

4.2. Influence of the Order of the Fractional Derivative α. Figures 5 and 6 show the influence of the parameter α on the development of excess pore pressure when the values of $\tau_\sigma/\tau_\varepsilon$ are 3.0 and 0.5, respectively. When $\tau_\sigma/\tau_\varepsilon = 3.0$, the excess pore pressure increases with the increase of α before the peak value. After the peak, the increase of α seems to accelerate the dissipation of the excess pore pressure. When $\tau_\sigma/\tau_\varepsilon = 0.5$, an opposite trend could be observed. With increasing α, the peak value of excess pore pressure shows a decreasing trend, and the after-peak dissipation rate is smaller. It can be seen that the influence of the fractional derivative parameter α on the development of excess pore pressure depends on the characteristics of the soil mass.

Figures 7 and 8 show the influence of the parameter α on the displacement development under the same conditions. Similar trends to that of the excess pore pressure can be observed. Another finding is that the influence of α is more

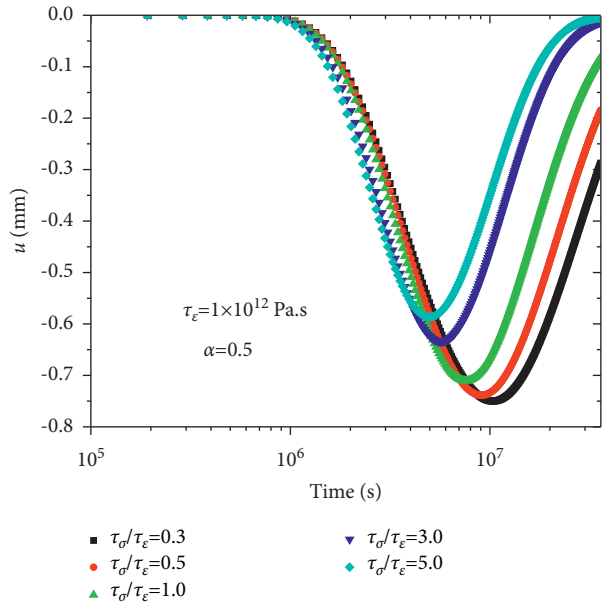

Figure 10: Influence of the material parameter $\tau_\sigma/\tau_\varepsilon$ on displacement when $\alpha = 0.5$.

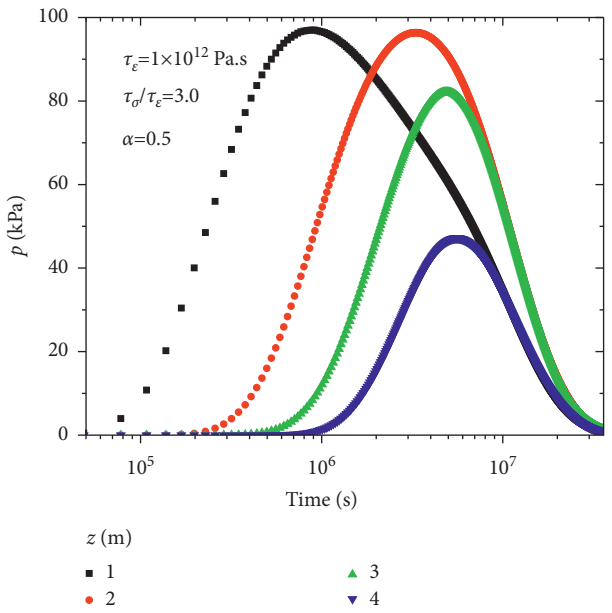

Figure 11: Influence of embedment depth on pore water pressure when $\tau_\sigma/\tau_\varepsilon = 3$.

obvious at $\tau_\sigma/\tau_\varepsilon = 3.0$. It can be seen that the soil property would influence the impact of the fractional derivative parameter on the development of displacement.

4.3. Influence of Material Parameters $\tau_\sigma/\tau_\varepsilon$. Figures 9 and 10 depict the influence of $\tau_\sigma/\tau_\varepsilon$ variance on the development of excess pore pressure and displacement with $\alpha = 0.5$. With increasing $\tau_\sigma/\tau_\varepsilon$, both the peak value of the excess pore value and the after-peak dissipation rate are much larger, while the net maximum displacement value decreases. The influence of $\tau_\sigma/\tau_\varepsilon$ on the trend of displacement development is less obvious.

The influence of embedment depth on the development of excess pore pressure and displacement is presented in Figures 11–14. As shown in Figures 11 and 12, the magnitude of excess pore pressure at $\tau_\sigma/\tau_\varepsilon = 3$ is much larger than that at $\tau_\sigma/\tau_\varepsilon = 0.5$. On the other hand, the development trend of excess pore pressure at different depths seems to be uninfluenced with the variance of $\tau_\sigma/\tau_\varepsilon$, but the peak excess pore pressure decreases with depth. As depicted in Figures 13 and 14, similar trends could be observed for the development of the displacement value. With increasing depth, the displacement value is much smaller.

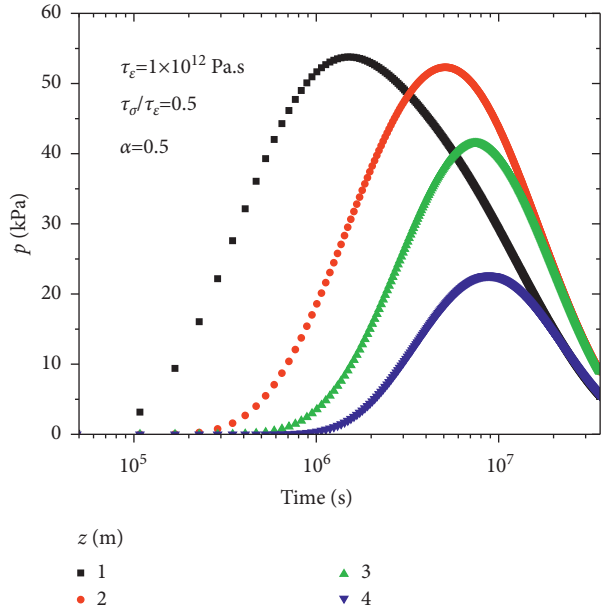

Figure 12: Influence of embedment depth on pore water pressure when $\tau_\sigma/\tau_\varepsilon = 0.5$.

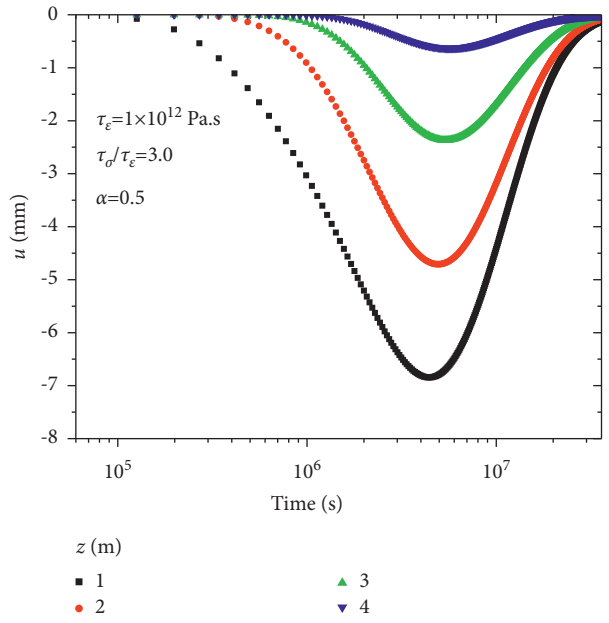

Figure 13: Influence of embedment depth on displacement when $\tau_\sigma/\tau_\varepsilon = 3$.

4.4. Influence of the Phenomenological Coefficient S_w. The influence of the phenomenological coefficient S_w on the development of excess pore pressure, displacement, and temperature increment is presented in Figures 15–17. It is clear that both the excess pore pressure and displacement increase with increasing S_w. On the other hand, the variance of S_w seems to have no impact on the development of temperature increment. This parametric analysis indicates

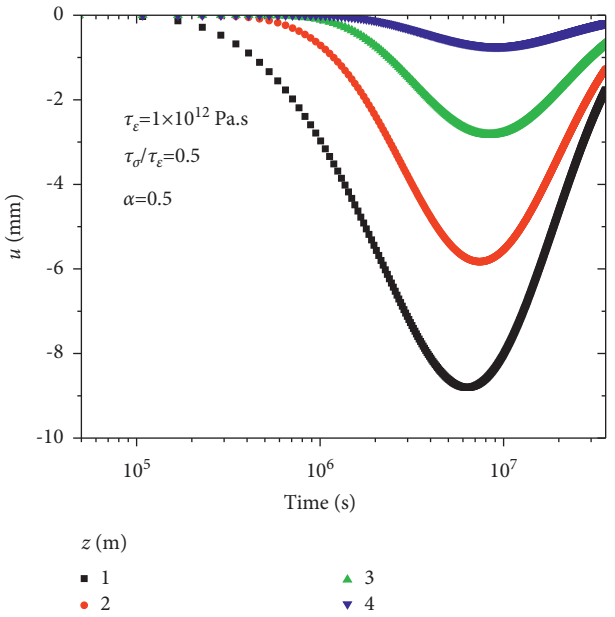

Figure 14: Influence of embedment depth on displacement when $\tau_\sigma/\tau_\varepsilon = 0.5$.

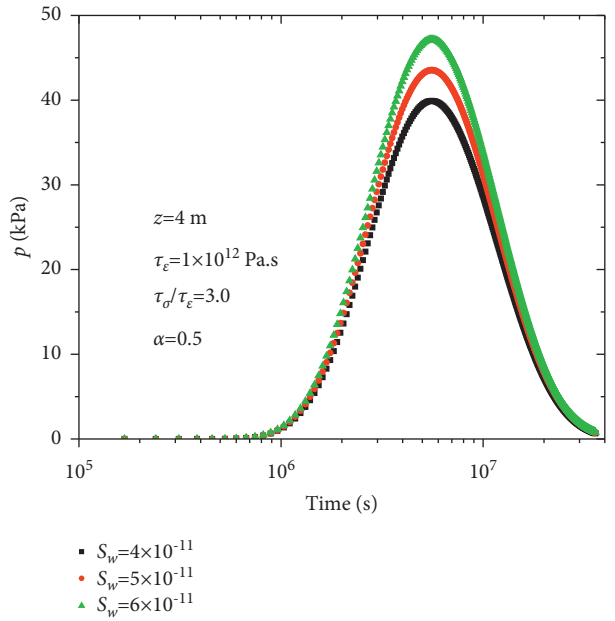

Figure 15: Influence of the phenomenological coefficient S_w on excess pore pressure.

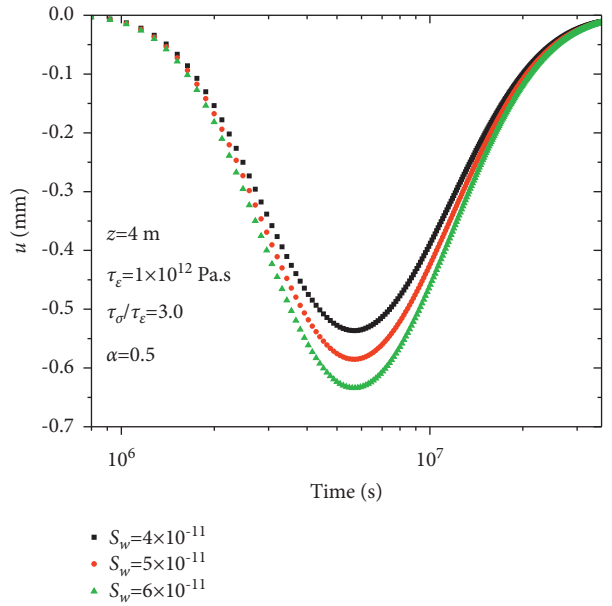

Figure 16: Influence of the phenomenological coefficient S_w on displacement.

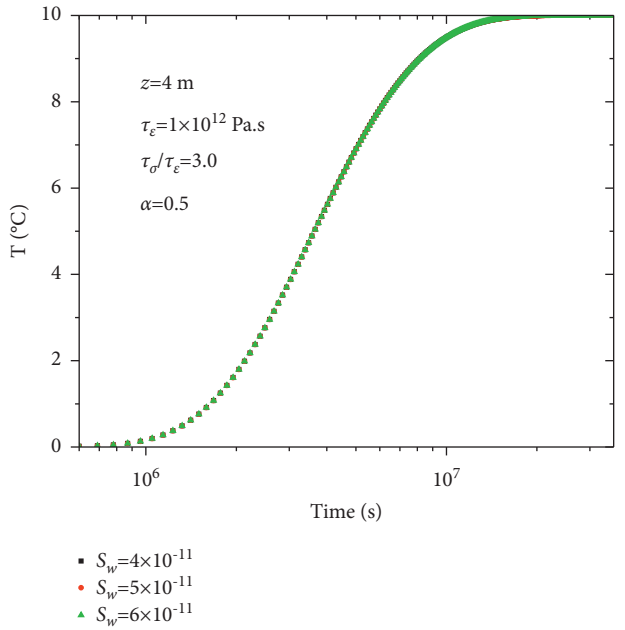

Figure 17: Influence of the phenomenological coefficient S_w on temperature increment.

that the thermal gradient has an obvious effect on the thermal filtration and thermo-osmosis process.

5. Conclusion

In this paper, a three-parameter fractional order derivative model is proposed based on the improved thermo-hydro-mechanical coupling theory by accounting for the viscoelastic behavior of marine clay. One-dimensional thermal consolidation of viscoelastic marine clay is analyzed, considering the thermal filtration and thermo-osmosis process. Solutions of excess pore pressure, temperature increment, and displacement are obtained by using the Laplace transform method and its numerical inverse transform. The influence of the order of the fractional derivative, material parameters, and phenomenological coefficient on the characteristics of thermal consolidation of marine clay is investigated. The performance of the proposed fractional derivative viscoelastic model (FDVM), Kelvin viscoelastic model (KVM), and elastic model (EM) is compared. The calculated excess pore pressure values from the three models are quite different, while the development of temperature increment seems to be uninfluenced by the selected model. For the development of the displacement value, there is an obvious turn of the displacement value for different models at the depth of 0.6 m. Further parametric analysis indicates that the influence of the fractional derivative parameter on the development of excess pore pressure and displacement depends on the properties of the soil mass, and the temperature increment has an obvious effect on the thermal filtration and thermo-osmosis process.

Data Availability

Data are available on request from the authors.

Conflicts of Interest

The authors declare that they have no conflicts of interest.

Acknowledgments

This research was supported by the National Natural Science Foundation of China (Grant nos. 52108347, 52178371), the Outstanding Youth Project of the Natural Science Foundation of Zhejiang Province (Grant no. LR21E080005), and the Exploring Youth Project of Zhejiang Natural Science Foundation (Grant no. LQ22E080010). The China Postdoctoral Science Foundation Funded Project (Grant no. 2020M673093) and the Construction Research Founds of Department of Housing and Urban-Rural Development of Zhejiang Province (Grant no. 2021K256), and the funds from the Engineering Research Center of Rock-Soil Drilling & Excavation and Protection, Ministry of Education (Grant No.202203) are also acknowledged.

References

[1] F. G. F. Gibb, "A new scheme for the very deep geological disposal of high-level radioactive waste," *Journal of the Geological Society*, vol. 157, no. 1, pp. 27–36, 2000.

[2] Y. N. Abousleiman and S. Ekbote, "Solutions for the inclined borehole in a porothermoelastic transversely isotropic medium," *Journal of Applied Mechanics*, vol. 72, no. 1, pp. 102–114, 2005.

[3] Y. P. Zhang, G. S. Jiang, W. B. Wu et al., "Analytical solution for distributed torsional low strain integrity test for pipe pile," *International Journal for Numerical and Analytical Methods in Geomechanics*, vol. 46, no. 1, pp. 47–67, 2022.

[4] Y. Man, H. X. Yang, N. R. Diao, J. H. Liu, and Z. H. Fang, "A new model and analytical solutions for borehole and pile ground heat exchangers," *International Journal of Heat and Mass Transfer*, vol. 53, no. 13-14, pp. 2593–2601, 2010.

[5] M. J. Wen, H. R. Xiong, and J. M. Xu, "Thermo-hydro-mechanical response of a partially sealed circular tunnel in saturated rock under inner water pressure," *Tunnelling and Underground Space Technology*, vol. 126, Article ID 104552, 2022.

[6] W. B. Wu, Z. J. Yang, X. Liu et al., "Horizontal dynamic response of pile in unsaturated soil considering its construction disturbance effect," *Ocean Engineering*, vol. 245, Article ID 110483, 2022.

[7] A. F. Rotta Loria and L. Laloui, "Thermally induced group effects among energy piles," *Géotechnique*, vol. 67, pp. 374–393, 2017.

[8] Y. P. Zhang, Z. Q. Wang, M. H. El Naggar, W. B. Wu, L. X. Wang, and G. S. Jiang, "Three-dimensional wave propagation in a solid pile during torsional low strain integrity test," *International Journal for Numerical and Analytical Methods in Geomechanics*, vol. 2022, 2022.

[9] Y. Tian, W. B. Wu, M. J. Wen, G. S. Jiang, M. H. El Naggar, and G. X. Mei, "Nonlinear consolidation of soft foundation improved by prefabricated vertical drains based on elliptical cylindrical equivalent model," *International Journal for Numerical and Analytical Methods in Geomechanics*, vol. 45, no. 13, pp. 1949–1971, 2021.

[10] Y. Tian, G. S. Jiang, W. B. Wu et al., "Elliptical cylindrical equivalent model of PVD-assisted consolidation under surcharge combined with vacuum preloading and its application," *Computers and Geotechnics*, vol. 139, Article ID 104389, 2021.

[11] M. F. Zong, Y. Tian, R. Z. Liang, W. B. Wu, M. J. Xu, and G. X. Mei, "One-dimensional nonlinear consolidation analysis of soil with continuous drainage boundary," *Journal of Central South University*, vol. 29, no. 1, pp. 270–281, 2022.

[12] D. L. Slegel and L. R. Davis, "Transient heat and mass transfer in soils in the vicinity of heated porous pipes," *Journal of Heat Transfer*, vol. 99, no. 4, pp. 541–546, 1977.

[13] M. J. Wen, Y. Tian, L. C. Li, K. H. Wang, and W. B. Wu, "An imperfect thermal contact problem for consolidation of bilayered saturated soil subjected to ramp-type heating," *International Journal of Heat and Mass Transfer*, vol. 190, Article ID 122755, 2022.

[14] J. C. Liu, W. T. Shi, and G. H. Lei, "Influence of viscosity on one-dimensional thermal consolidation of marine clay," *Marine Georesources & Geotechnology*, vol. 37, no. 3, pp. 331–338, 2019.

[15] M. A. Biot, "Thermoelasticity and irreversible thermo-dynamics," *Journal of Applied Physics*, vol. 27, no. 3, pp. 240–253, 1956.

[16] J. R. Booker and C. Savvidou, "Consolidation around a spherical heat source," *International Journal of Solids and Structures*, vol. 20, no. 11-12, pp. 1079–1090, 1984.

[17] J. R. Booker and C. Savvidou, "Consolidation around a point heat source," *International Journal for Numerical and*

Analytical Methods in Geomechanics, vol. 9, no. 2, pp. 173–184, 1985.

[18] B. Bai, "Fluctuation responses of saturated porous media subjected to cyclic thermal loading," *Computers and Geotechnics*, vol. 33, no. 8, pp. 396–403, 2006.

[19] D. W. Smith and J. R. Booker, "Green's functions for a fully coupled thermoporoelastic material," *International Journal for Numerical and Analytical Methods in Geomechanics*, vol. 17, no. 3, pp. 139–163, 1993.

[20] Z. Lu, H. L. Yao, and G. B. Liu, "Thermomechanical response of a poroelastic half-space soil medium subjected to time harmonic loads," *Computers and Geotechnics*, vol. 37, no. 3, pp. 343–350, 2010.

[21] Z. Y. Ai and L. J. Wang, "Axisymmetric thermal consolidation of multilayered porous thermoelastic media due to a heat source," *International Journal for Numerical and Analytical Methods in Geomechanics*, vol. 39, no. 17, pp. 1912–1931, 2015.

[22] Z. Y. Ai, Z. Ye, Z. Zhao, Q. L. Wu, and L. J. Wang, "Time-dependent behavior of axisymmetric thermal consolidation for multilayered transversely isotropic poroelastic material," *Applied Mathematical Modelling*, vol. 61, pp. 216–236, 2018.

[23] M. J. Wen, J. M. Xu, and H. R. Xiong, "Thermo-hydro-mechanical dynamic response of a cylindrical lined tunnel in a poroelastic medium with fractional thermoelastic theory," *Soil Dynamics and Earthquake Engineering*, vol. 130, Article ID 105960, 2020.

[24] R. C. Srivastava and P. K. Avasthi, "Non-equilibrium thermodynamics of thermo-osmosis of water through kaolinite," *Journal of Hydrology*, vol. 24, no. 1-2, pp. 111–120, 1975.

[25] Y. Zhou, R. K. N. D. Rajapakse, and J. Graham, "A coupled thermoporoelastic model with thermo-osmosis and thermal-filtration," *International Journal of Solids and Structures*, vol. 35, no. 34–35, pp. 4659–4683, 1998.

[26] G. B. Liu, K. H. Xie, and R. Y. Zheng, "Model of nonlinear coupled thermo-hydro-elastodynamics response for a saturated porous medium," *Science in China, Series A: Technological Sciences)*, vol. 52, pp. 2373–2383, 2009.

[27] G. B. Liu, K. H. Xie, and R. Y. Zheng, "Thermo-elastodynamic response of a spherical cavity in saturated poroelastic medium," *Applied Mathematical Modelling*, vol. 34, no. 8, pp. 2203–2222, 2010.

[28] Y. Yang, K. Guerlebeck, and T. Schanz, "Thermo-osmosis effect in saturated porous medium," *Transport in Porous Media*, vol. 104, no. 2, pp. 253–271, 2014.

[29] J. C. Liu, G. H. Lei, and X. D. Wang, "One-dimensional consolidation of visco-elastic marine clay under depth-varying and time-dependent load," *Marine Georesources & Geotechnology*, vol. 33, no. 4, pp. 337–347, 2015.

[30] L. J. Wang and L. H. Wang, "Semianalytical analysis of creep and thermal consolidation behaviors in layered saturated clays," *International Journal of Geomechanics*, vol. 20, no. 4, Article ID 06020001, 2020.

[31] H. H. Zhu, C. C. Zhang, G. X. Mei, B. Shi, and L. Gao, "Prediction of one-dimensional compression behavior of Nansha clay using fractional derivatives," *Marine Georesources & Geotechnology*, vol. 35, no. 5, pp. 688–697, 2017.

[32] L. C. Li, X. Liu, H. Liu et al., "Experimental and numerical study on the static lateral performance of monopile and hybrid pile foundation," *Ocean Engineering*, vol. 255, Article ID 111461, 2022.

[33] L. C. Li, M. Y. Zheng, X. Liu et al., "Numerical analysis of the cyclic loading behavior of monopile and hybrid pile foundation," *Computers and Geotechnics*, vol. 144, Article ID 104635, 2022.

[34] M. H. Huang and J. C. Li, "Consolidation of viscoelastic soil by vertical drains incorporating fractional-derivative model and time-dependent loading," *International Journal for Numerical and Analytical Methods in Geomechanics*, vol. 43, no. 1, pp. 239–256, 2018.

[35] L. Wang, D. A. Sun, P. C. Li, and Y. Xie, "Semi-analytical solution for one-dimensional consolidation of fractional derivative viscoelastic saturated soils," *Computers and Geotechnics*, vol. 83, pp. 30–39, 2017.

[36] Y. A. Rossikhin and M. V. Shitikova, "Applications of fractional calculus to dynamic problems of linear and nonlinear hereditary mechanics of solids," *Applied Mechanics Reviews*, vol. 50, no. 1, pp. 15–67, 1997.